Pure Appl. Chem., Vol. 78, No. 9, pp. 1651–1665, 2006.
doi:10.1351/pac200678091651

Nanorods of CoP, CdS, and ZnS*

P. John Thomas, Paul Christian, Steven Daniels, Yang Li, Y. S. Wang†, and Paul O'Brien‡

School of Chemistry, The University of Manchester, Oxford Road, Manchester, M13 9PL, UK

Abstract: Simple thermolysis routes to CdS, ZnS, and CoP nanorods have been developed in our laboratory. The structural properties of the nanorods obtained were elucidated by means of X-ray diffraction (XRD) and high-resolution transmission electron microscopy (HR-TEM). Arguments and calculations in support of the contention that intrinsic rather than extrinsic factors influence the solution-phase growth of nanorods are presented.

Keywords: nanorods; nanowires; crystal growth; nanomaterials; nanocrystals; particle synthesis.

INTRODUCTION

Nanowires, nanorods, and other nanodimensional material have been intensely researched in recent years because of their unique properties. At nanometric sizes, quantum confinement effects can come into play and affect most notably the electronic properties [1]. The growth of interest in this area has furthered our understanding of natural phenomena and has paved the way for building nanodevices with potential to impact our everyday life.

A key step in the advance of nanoscience is devising synthetic strategies to yield nanodimensional matter with good control over shape and size. Nanorods and nanowires of metals, chalcogenides, and oxides have been obtained by different methods [2]. Many of these methods rely on templates such as porous alumina to direct the growth. There are some examples of solution-phase methods of growing nanowires or nanorods without the use of any template. CdS nanorods have been obtained by thermolysis of single-source precursors such as xanthates ($Cd(C_2H_5OCS_2)_2$) [3], dithiocarbamates ($Cd(S_2CNEt_2)_2$) [4], and thiosemicarbazide ($Cd[NH_2CSNHNH_2]_2Cl_2$) [5] in coordinating solvents at temperatures in the range of 120–300 °C. The CdS nanorods thus produced adopt the hexagonal wurtzite form. Nanorods of magnetic Fe, Co, and Ni phosphides have been synthesized by a thermolysis process involving sequential or continual injection of metal-triphenylphosphine complex into a hot coordinating solvent mixture [6,7]. ZnS nanorods have been obtained in aqueous solution by the use of a liquid crystal as template [8]. Building on our experience with solution-phase synthesis of semiconducting nanocrystalline material, we have developed simple synthetic routes to semiconductor nanorods. In this paper, we report on the synthesis of CdS, ZnS, and CoP nanorods. The structural properties of the nanorods obtained were elucidated by means of X-ray diffraction (XRD) and high-resolution transmission electron microscopy (HR-TEM). We also present arguments and calculations in sup-

*Paper based on a presentation at the 3rd IUPAC Workshop on Advanced Materials (WAM III), Stellenbosch, South Africa, 5–9 September 2005. Other presentations are published in this issue, pp. 1619–1801.

†Permanent address: Department of Physics, Beijing Normal University, Beijing 1000875, P.R. China
‡Corresponding author: E-mail: paul.obrien@manchester.ac.uk

port of the contention that intrinsic rather than extrinsic factors influence the solution-phase growth of nanorods.

EXPERIMENTAL

CoP nanorods

In a typical reaction, a vigorously stirred mixture of hexadecylamine (HDA) (15 g, 98 %) and tri-*n*-octylphosphineoxide (TOPO) (15 g, 99 %) under vacuum was kept at 140 °C for 1 h to remove water. The mixture was cooled to 100 °C, and cobaltacetylacetonate (0.128 g, 0.5 mmol) and tetradecylphosphonic acid (TDPA) (0.5 g, 98 %) were added and stirred magnetically under a flow of nitrogen. The temperature was slowly increased to 340 °C over 1 h, and the solution was maintained at this temperature for 3 h. The color of the solution changed from an initial transparent violet to turbid dark brown. The solution was then allowed to cool to 60 °C. An excess of ethanol was added to the solution to give a black precipitate, which was separated by centrifugation and dried under vacuum. The black powder could easily be redispersed in organic solvents, such as chloroform, hexane, and toluene. Experiments were carried out with different weight ratios of HDA and TOPO and at different temperatures.

CdS nanorods

Anhydrous cadmium acetate was dissolved in octylamine (10 ml). A stoichiometric amount of sulfur was dissolved in octylamine (10 ml). In a typical reaction, HDA (100 g) was degassed under reduced pressure for 1 h at 140 °C then brought up to atmospheric pressure under nitrogen. The reaction mixture was held at 140 °C, and the sulfur-containing solution (1 ml) injected followed by the cadmium acetate solution (1 ml). The reaction was left to proceed for 15 min, after which the remaining reagents were added at a rate of 3.17 ml/h over approximately 3 h. The reaction mixture was then maintained at 140 °C for a further 10 h. After cooling, the particles were precipitated by the addition of dry methanol and isolated by centrifugation. The product was then redissolved in toluene and reprecipitated with methanol. Reactions were carried out with different concentrations of cadmium acetate.

ZnS nanorods

In a typical reaction, 100 g HDA was degassed at 120 °C for 1 h, and then heated under nitrogen to 140 or 180 °C. Two separate dropping funnels containing solutions of sulfur (1 g, 0.32 mol) in octylamine (30 ml) and zinc acetate dihydrate (3.18 g, 0.32 mol) in octylamine (30 ml) were used to control the addition of the precursors. 1 ml of the zinc stock solution was added followed by 1 ml of the sulfur stock solution under vigorous stirring, and the mixture was kept at 140 °C for 30 min. The rest of the stock solutions were then added simultaneously at the same temperature over a period of 20 min. After complete addition, the solution was stirred for a further 2 h. Then the solution was cooled to 80 °C and the ZnS nanorods were precipitated by the addition of excess ethanol and washed three times with acetone to remove unreacted residuals.

Characterization

X-ray powder diffraction studies were conducted on a Bruker D8 AXS diffractometer using monochromated Cu-Kα radiation or a Philips PW 3020 with Co-Kα radiation with a Fe filter. Samples were prepared by depositing the nanorods solids on either glass or Si substrates. TEM analyses were carried on Philips CM200, 200KV DX4EDS and Technai FEG-TEM 300 kV microscopes. Samples were dissolved in toluene and filtered, and a drop of the nanorod solution was then placed on a TEM grid and

allowed to dry. Photoluminescence spectra were measured using a Horiba Fluorolog-3 (FL3-22) spectrometer. Luminescence measurements were carried out using samples dispersed in chloroform.

RESULTS AND DISCUSSION

CoP nanorods

A typical XRD pattern from the black solid obtained by decomposing cobalt acetylacetonate and HDPA in TOPO/HDA mixture under the conditions detailed above are shown in Fig. 1. All the prominent peaks in the pattern can be matched to orthorhombic CoP (JCPDS No: 29-0497). The unit cell dimensions were determined from the above pattern by Rietveld analysis and were found to be a = 0.5074 nm and c = 0.3279 nm. The unit cell dimensions closely match the reported values of a = 0.5077 nm and c = 0.3281 nm.

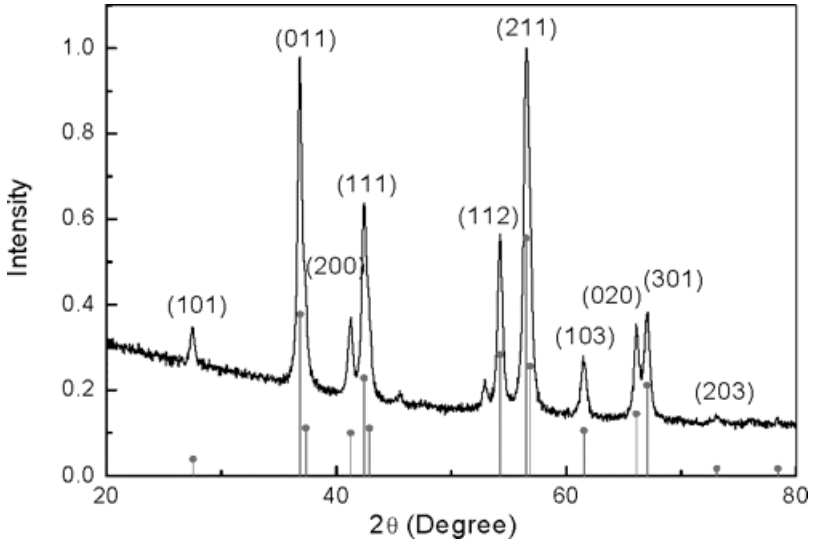

Fig. 1 XRD pattern of the sample obtained using HDA:TOPO weight ratio of 1:1. The peaks corresponding to the standard pattern of orthorhombic CoP (JCPDS No: 29-0497) are shown.

TEM images of CoP samples obtained using HAD:TOPO weight ratios of 1:1 and 1:2 are shown in Fig. 2. The images reveal that the samples are exclusively made of nanowires with a uniform diameter and length. The nanowires that obtained a HDA:TOPO ratio of 1:2 were found to be ~10 nm in diameter and 100 ± 10 nm in length (Fig. 2A). An increase in the amount to HDA (HAD:TOPO weight ratio 1:1) leads to an increase in the length of nanowires, accompanied by a small decrease in the diameters of the nanowires. The nanowires obtained with a HDA:TOPO ratio of 1:2 are 7 nm in diameter and 400 ± 20 nm in length (Fig. 2B). Clearly, the weight ratio of the constituent solvents plays a key role in determining the dimensions of the nanowires. It is noteworthy that the nanowires tend to form an ordered arrangement with the long axes parallel to one another, perhaps due to their magnetic nature. Reactions carried out with pure TOPO or pure HDA as solvent yield no nanowires. A mixed reaction system consisting of TOPO and HDA is essential for promoting anisotropic growth.

Reaction temperature is another key factor in the formation of the CoP nanowires. The reaction temperature has to be sufficiently high to cleave the bonds between carbon and phosphorus in the alkylphosphonic acid (TDPA) to enable it to act as a phosphide source [9–11]. We found that temperatures in excess of 320 °C suffice to cleave the bonds and facilitate the formation of CoP. At tempera-

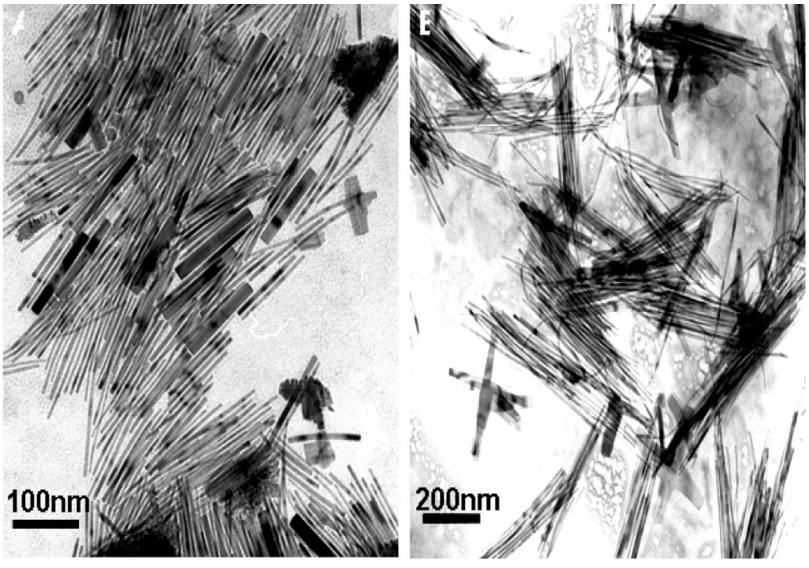

Fig. 2 TEM images of CoP nanowires prepared with HDA:TOPO weight ratios of (A)1:2 and (B)1:1.

tures lower than 320 °C, no CoP was obtained. We also have found that CoP nanostructures can only be prepared from phosphonic acids with long-chain carbon substituents; the methyl or ethylphosphonic acids are more thermally stable.

It is well known that technical-grade TOPO contains alkylphosphonic acids as impurities [12,13]. We found that replacing pure TOPO and TDPA with technical-grade TOPO (15 g, 90 %, Aldrich) also yields CoP nanowires. Thus, unpurified TOPO can serve as an effective capping agent and phosphorus source. This observation is significant as pure TOPO and alkylphosphonic acid are much more expensive than crude TOPO.

HR-TEM helps us understand the structure of nanowires. The HR-TEM image and a diffraction pattern obtained from a CoP nanowire with diameter of 7 nm are shown in Fig. 3. The regularity of the lattice planes in the HR-TEM image (Fig. 3A) indicates that the CoP nanowires are single-crystalline. The spacing between adjacent fringes is 0.283 nm and corresponds to the (011) planes of orthorhombic CoP. The preferred orientation of nanowires is parallel to the (011) plane. Further evidence for the single-crystalline nature of the nanowires could be obtained from the power spectrum of the HR-TEM image obtained by fast Fourier diffraction, which reveals clear spots that can be matched with the characteristic pattern associated with the wurtzite-orthorhombic crystalline structure of CoP. The reciprocal lattice peaks obtained from the power spectrum are compatible with a lattice constant of 0.289 nm. Selected area electron diffraction (SAED) patterns reveal diffuse rings (Fig. 3B) that can be indexed to (011), (111), (211), (103), and (301) planes of the orthorhombic CoP.

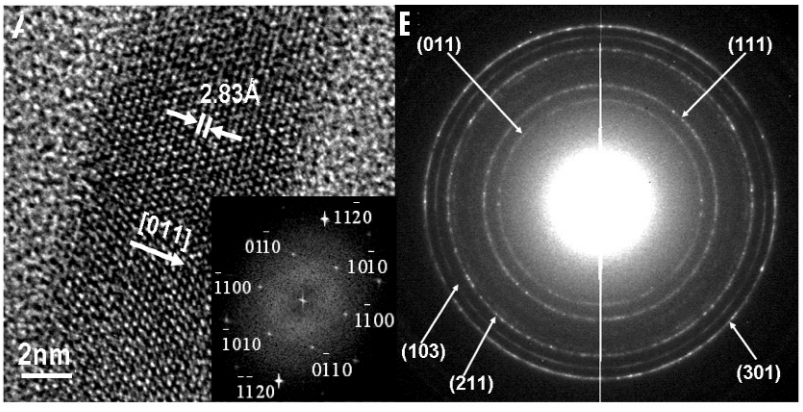

Fig. 3 (A) HR-TEM image of a 7-nm-diameter CoP nanowire. The inset shows a fast Fourier transform of the HR-TEM image. (B) SAED pattern from an assembly of CoP nanowires.

CdS nanorods

Four samples (A–D) were prepared using different concentrations of cadmium acetate. The concentrations used and related properties of the samples are summarized in Table 1. Typical XRD patterns of samples A and B are shown in Fig. 4. The patterns reveal that the phase of CdS is dependent on the concentration of the cadmium source employed. At low concentrations (sample A), CdS is present in the thermodynamically stable hexagonal phase. X-ray pattern reveals that a 70 % increase in the concentration of Cd source results in a dramatic collapse of the hexagonal phase and emergence of the cubic phase. The above indication from XRD is suggestive rather than conclusive. The peaks in the diffraction patterns of nanocrystalline samples are broadened by the finite size effects. Furthermore, the similarities in the pattern between cubic and hexagonal forms of CdS thwart unequivocal phase assignments in these cases. Despite these limitations, we believe that the change in phase indicated by the X-ray patterns do correspond to a phase change, since similar reaction conditions were for preparing both samples. It is possible that sample B is polytypical with a cubic phase being predominant. We believe that a change in the predominant phase to cubic results from a more rapid reaction due to the more concentrated solution.

Table 1

Sample	Quantity of $Cd(ac)_2$ mmol	Final concn. M
A	1.3	0.011
B	2.2	0.018
C	21.7	0.181
D	31.6*	0.198

*Added as three injections of 10 ml.

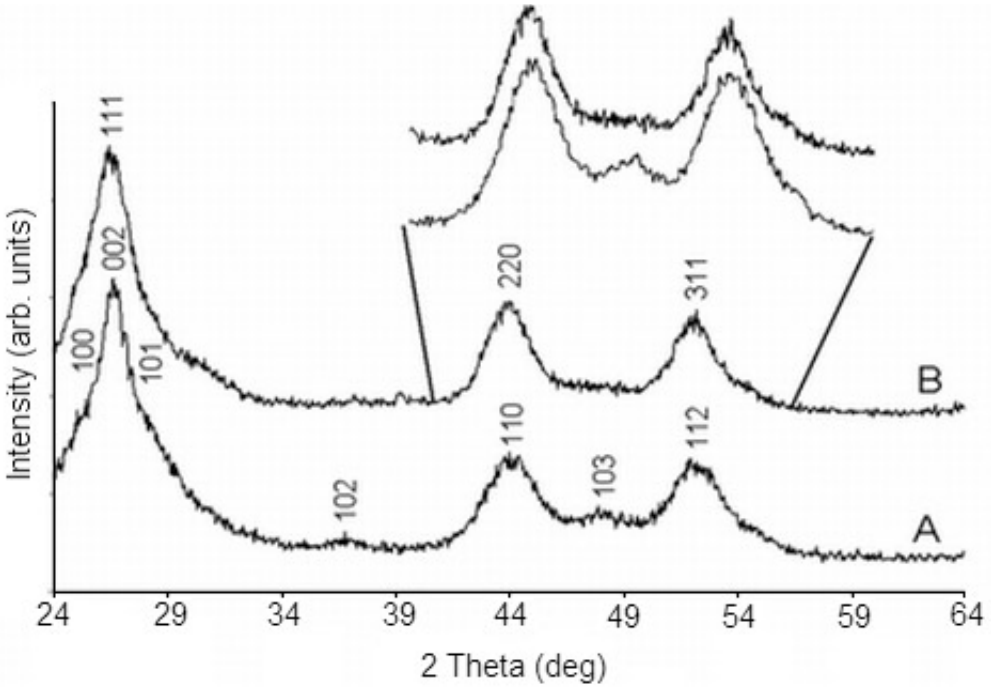

Fig. 4 XRD patterns showing the hexagonal phase of sample A and cubic phase of sample B. The inset is at higher resolution.

TEM images reveal interesting changes in the morphology of the samples (see Fig. 5). Sample A, corresponding to the lowest concentration consists of large numbers of spherical particles with diameters of 3.5 nm. At the highest concentration (sample D), nanorods with diameters of ~7 nm and lengths of ~25 nm as well as nanocrystals with diameters of ~7 nm are seen. At intermediate concentrations, nanocrystals and nanorods with diameters of 4 nm (sample B) and 6.5 nm (sample C) are present. Nanorods are seen in all samples, but their abundances vary with concentration. Nanorods constitute 72 % of sample D. Sample C was made up of ~15 % nanorods. The percentage of nanorods was less than 5 % in samples A and B. Optical bandgaps of the dispersions were obtained by extrapolation of the absorption onsets. The bandgaps shift to red with increase in concentration. Sample A has a bandgap of 446 nm, while sample D possesses a bandgap of 481 nm.

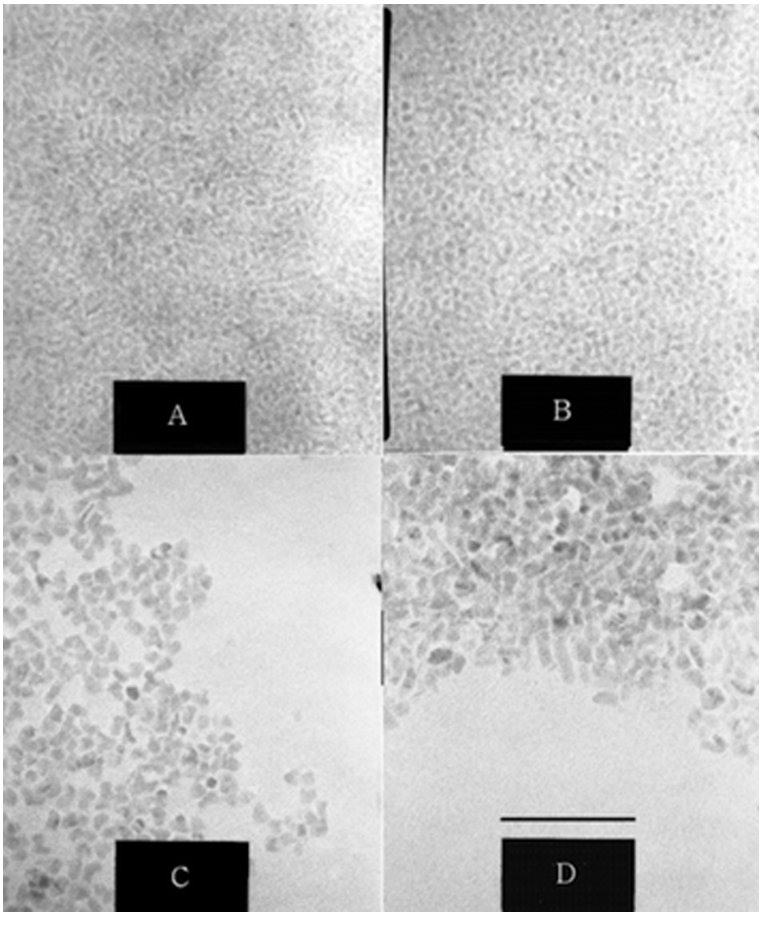

Fig. 5 TEM images of samples A–D. Scale bar shows 85 nm.

All the samples were luminescent (see Fig. 6). The emission peaks exhibit a red shift with increase in concentration, reflecting the change in the optical bandgaps. The emission maximums are sample A: 465 nm, sample B: 489 nm, sample C: 599 nm, sample D: 504 nm. The quantum yield varied from 2.3–0.1 % with no apparent trend.

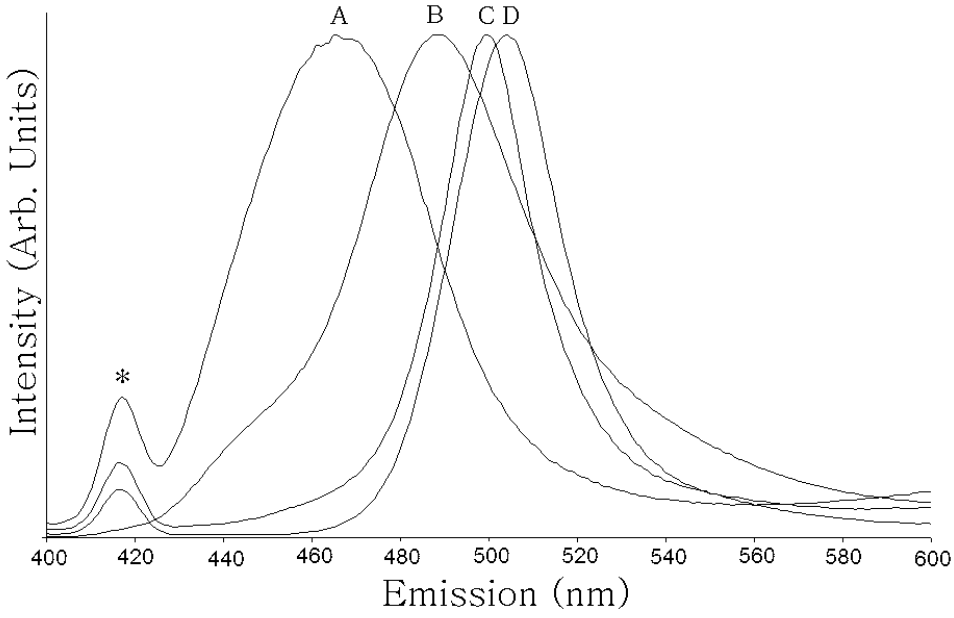

Fig. 6 Photoluminescence spectra for samples A–D, excited at 380 nm (* indicates Raman scattering from solvent).

We were intrigued by the cubic phase adopted by the nanorods since almost all previously synthesized CdS nanorods are hexagonal [3–5,8]. Close inspection of the structure of the nanorods by HR-TEM reveals a more complicated picture. The cubic and hexagonal forms of CdS share similar lattice spacings for the (111) and (002) planes of 0.336 nm. However, the (100) plane for the hexagonal form is significantly larger (0.359 nm). Analysis of the lattice spacing of sample D by HR-TEM demonstrates the unperturbed 3.34-nm lattice spacing perpendicular to the long axis of the rod (Fig. 7, top). This is consistent with both the cubic (111) and hexagonal (002) planes (Fig. 7, center). However, lattice planes running parallel to the long axis show significant variations. Measurements at several points show a combination of lattice spacings of 0.333 and 0.352 nm (±0.005 nm). Thus, the nanorods rather than being single-crystalline consist of a mixture of the cubic and hexagonal phases. However, given the absence of reflection corresponding to the (103) plane in the XRD pattern, it seems plausible that the cubic phase is the dominant form in samples B, C, and D. These results are best rationalized as being due to a change in control of the reaction from close to thermodynamic at the lower concentrations to a kinetic regime at higher temperatures.

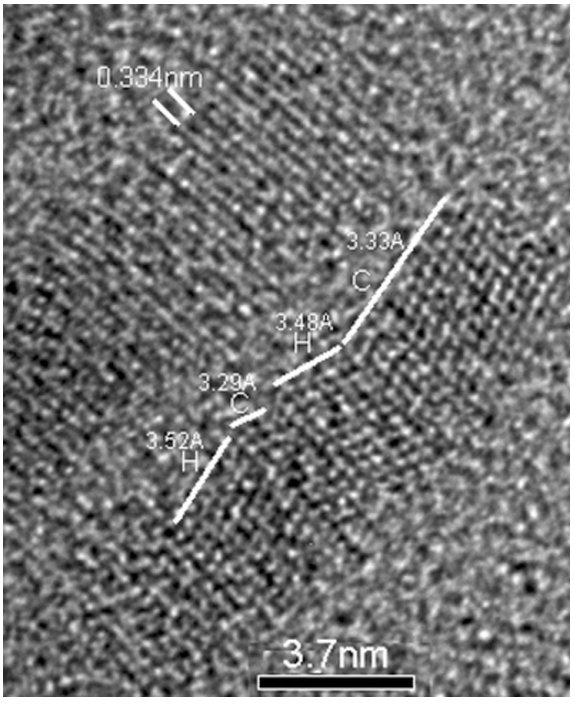

Fig. 7 HR-TEM image of a nanorod from sample D showing lattice spacing and hexagonal (H) and cubic (C) phases.

ZnS nanorods

The method employed for the synthesis of ZnS nanorods was inspired by the synthesis of CdS nanorods. We find that the phase of the material prepared depended on the reaction temperature. XRD of the materials prepared at low temperatures (140 °C) showed the ZnS to be a mixture of wurtzite and zinc blende, whereas the sample obtained at high temperature (180 °C) was found to be cubic phase. As in the case of CdS, the cubic and hexagonal phases have quite similar XRD patterns. Further, the peaks are broadened due to finite size effects making phase assignment inconclusive. However, the presence of a peak at 38º and the absence of a peak at 53º strongly suggest the presence of cubic phase. Rietveld analysis of the diffraction patterns suggests that the low-temperature sample was made up of a mixture of hexagonal and cubic phases, with a slight mismatch attributable to either a large number of cubic dislocations or orientation of the rods in the sample holder (see Fig. 8). The high-temperature sample was found to consist of a pure cubic phase. The most stable form of zinc sulfide is the cubic zinc blend phase, and it is therefore not surprising that the cubic phase is obtained at higher temperatures. However previous studies of bulk zinc sulfide have shown that the phase of the material is particularly dependent on the reaction conditions with the hexagonal phase being dominant at temperatures much lower than would be expected from a purely thermodynamic viewpoint [14].

TEM images reveal that sample obtained at low temperature consists of exceedingly fine nanorods (see Fig. 8). The average diameter of rods is 1.9 ± 0.2 nm, and the length is 23 ± 3 nm. An HR-TEM image of individual nanorods reveals regularly spaced lattice fringes with separation distance of 0.31 nm consistent with the spacing between (002) lattice planes. Thus, the nanorods are indeed single-crystalline. We found that the zinc sulfide crystallites grown at 180 °C are spherical, with average diameters of 7.5 ± 1 nm.

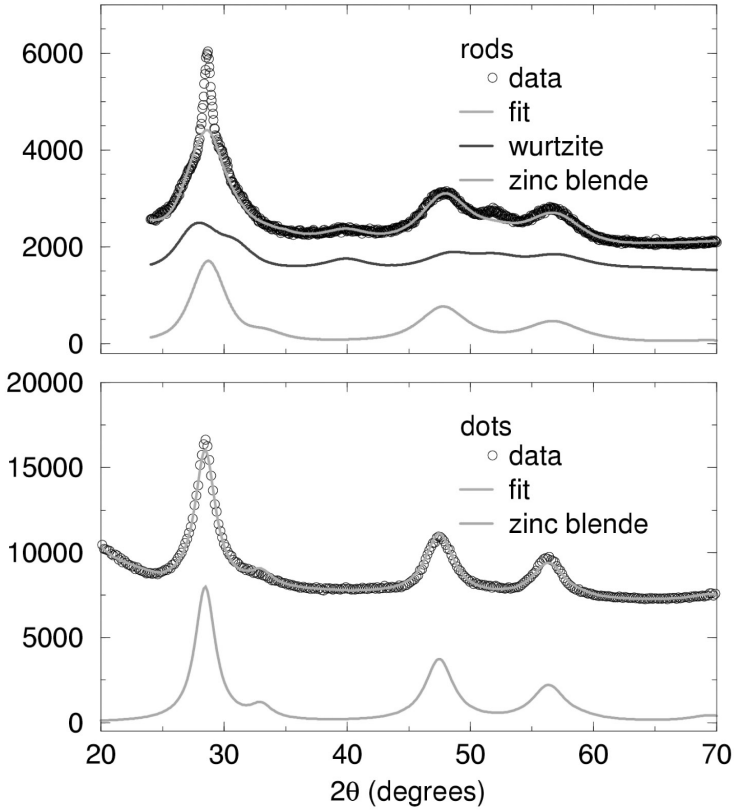

Fig. 8 XRD patterns of ZnS samples obtained at 140 °C (top) and at 180 °C (bottom). Fitted wurtzite and zinc blende fits are also shown.

The UV/vis spectra of the nanorods grown at 140 °C and nanodots grown at 180 °C are shown in Fig. 9. The onset of the absorption changes from 300 nm for the nanorods to 320 nm for the dots. The nanorods, therefore, have a higher bandgap than the nanocrystals.

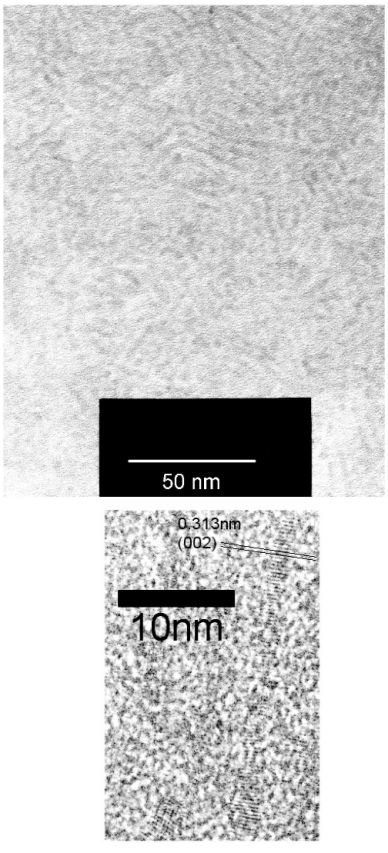

Fig. 9 TEM image of ZnS nanorods obtained at 140 °C (top). An HR-TEM image of a single ZnS nanorod is shown at the bottom.

Fundamental factors influencing the growth of nanorods

In the solution phase, nanorods of semicondutors and metals have been obtained using a variety of reagents under a multitude of conditions without the use of any templates. In this light, we considered it likely that intrinsic rather than extrinsic factors determine anisotropic growth of nanomaterials. We were also inspired by the success of the concept of magic numbers in the formation of noble gas and metal clusters. We have modeled the anisotropic growth of rods based simply on the number of atoms in the structure to see if anisotropic growth becomes favorable in certain size regime. The end result of the calculation is plot that is a landscape for anisotropic growth based on percentage of surface atoms (SAPs).

In our model, nanorods were assumed to grow out of a tetrahedral seed, which follows cubic close packing (CCP). The growth of the seed stops once the rods start growing. Rods follow either cubic or hexagonally close packed schemes and have either a triangular or hexagonal morphology. The assumptions were made based on structural observations obtained from tetrapods of chalcogenide nanocrystals. The number of surface atoms was calculated for each configuration using an iterative process, which arrives at individual configurations by layer-by-layer stacking of atoms. The changes in the SAPs accompanying the growth of a triangular rod from a tetrahedral seed of two different sizes are shown in Fig. 10. Perhaps contrary to intuition, we see that the growth of rod actually results in a drop in the SAPs. Such a drop means that growth of rod from the face of the seed reduces the internal energy. Thus, the need to conserve the number of surface atoms could provide impetus to an anisotropic growth

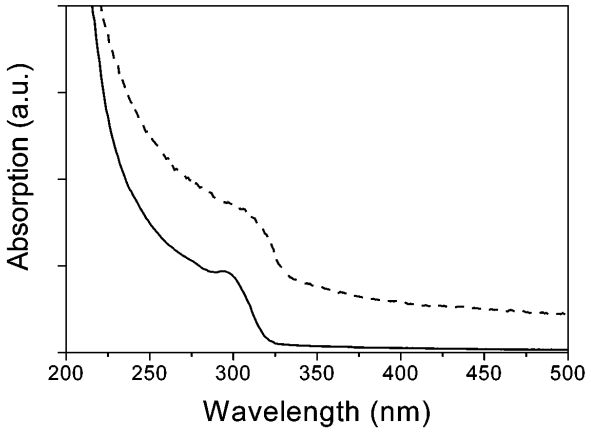

Fig. 10 Electronic absorption spectra of ZnS nanorods grown at 140 °C (solid line) and ZnS nanocrystals grown at 180 °C (dashed line).

process. In order to compare the growth of rods at different sizes, a characteristic change in the SAPs was sought to be associated with rods of different sizes. We believe that ΔSAP_{max}, the maximum gain in the percentage of surface atoms accompanying the growth of the branch of a particular size, could provide a quantity that is a measure of relief in internal energy accompanying the growth of nanorods. In other words, we assume that ΔSAP_{max} is directly proportional to the gain in internal energy. The changes in the ΔSAP_{max}, accompanying the growth of triangular and hexagonal rods following either the cubic or hexagonal close packing (HCP) schemes are shown in Fig. 11. The dimensions of the nanorods were estimated assuming that the material was CdS. It is seen that the growth of triangular CCP branches succeed in producing the maximum ΔSAP_{max} of 6.5 % at a size of ~3 nm. Such a difference in ΔSAP_{max} is indeed highly significant. Major changes in morphology are triggered by lesser differences in the fraction of surface atoms [15–18]. ΔSAP_{max} is strongly size-dependent, suggesting that the anisotropic growth of nanorods is fundamentally size-selective with certain favored sizes. In a real growth process, the solubility of the growing seed is an important factor which can influence the population of seeds and could bring in its own size-dependence. For that reason, the plots in Fig. 11 are only to be taken as broad indicators of the size-regime in which anisotropic growth processes are thermodynamically favored.

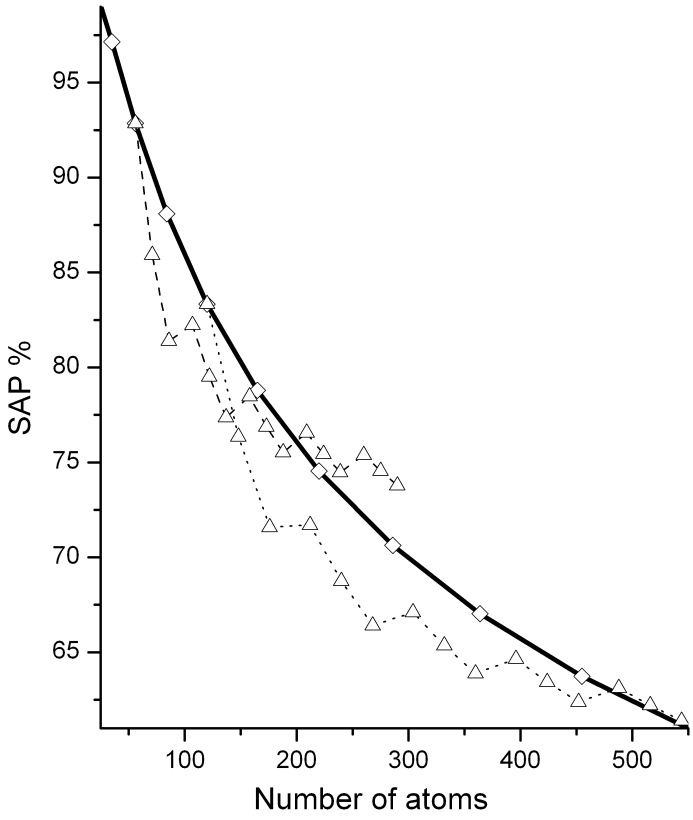

Fig. 11 Plot showing the changes in the SAP accompanying the growth of a triangular rod out of a tetrahedral seed at different nuclearities. The seed is indicated by a solid line, while the branches are indicated with dotted lines. The dimensions of the triangular rods are the same as that of the triangular face of the tetrahedral seed.

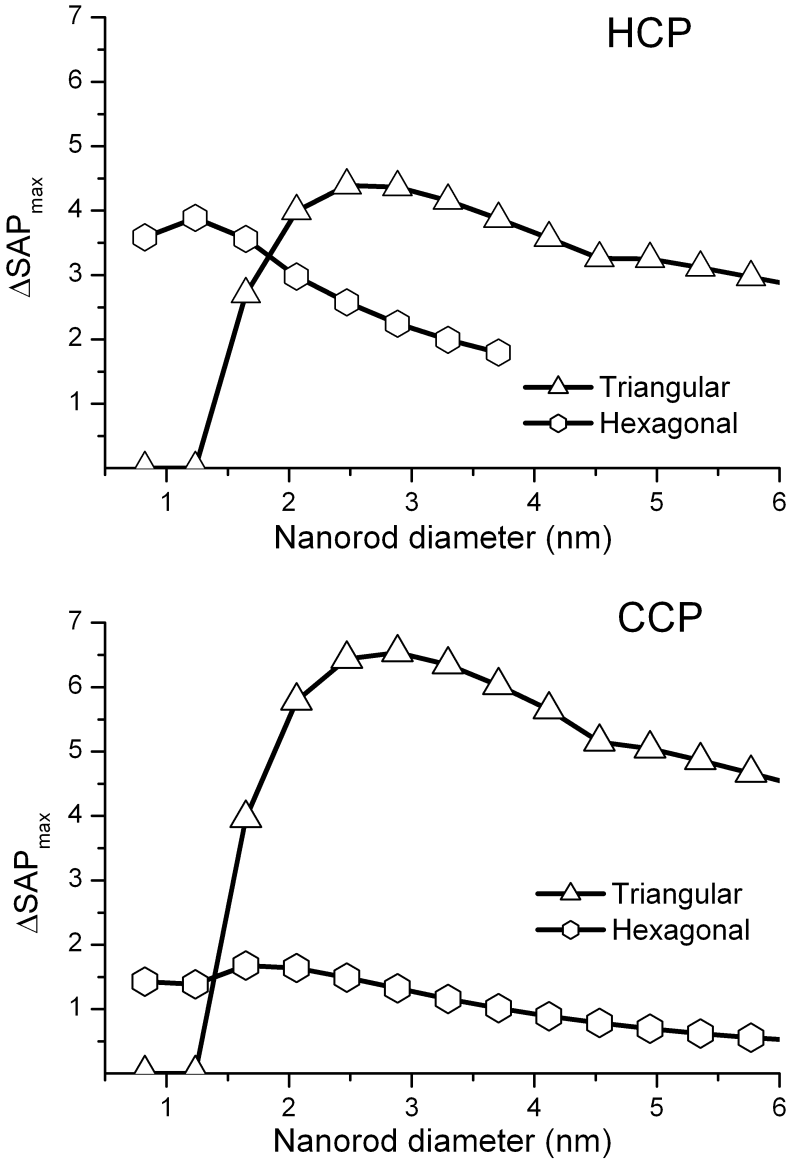

Fig. 12 Plot showing the ΔSAP_{max} that can be associated with rods of different morphologies growing out of a tetrahedral seed. The plots at the top correspond to rods adopting a CCP, while the ones at the bottom correspond to HCP. The dimensions of the triangular rods are the same as that of the triangular face of the tetrahedral seed. The hexagonal rod's dimensions correspond to the largest hexagon that can be fitted on the triangular face of the tetrahedral seed. The seed always adopts CCP. The nanorod diameters were arrived at considering the lattice constants of CdS.

CONCLUSIONS

A simple method employing $Co(acac)_2$ and long-chain alkylphosphonic acid in the presence of HDA and TOPO at high temperatures has been developed to synthesize CoP nanowires with a high aspect ratio. Technical grade TOPO can be a replacement for the combination of alkylphosphonic acid and pu-

rified TOPO in the synthetic scheme. The length and diameter of the nanowires can be varied by changing the HAD:TOPO ratio.

Predominantly cubic CdS nanowires were obtained by the use of simple precursors such as cadmium acetate and S. The morphology of the nanocryatalline matter produced is strongly dependent on the concentration of the reagents, with rods being the dominant product at high concentrations. This method can be extended to prepare single-crystalline ZnS nanorods.

Fundamental factors such as the need to conserve the number of surface atoms could provide a driving force for anisotropic growth processes producing nanorods. The change in the percentage of surface atoms accompanying the growth of nanorods from a seed is strongly size-dependent and is broadly indicative of a size-regime in which anisotropic growth is thermodynamically favorable.

REFERENCES

1. C. N. R. Rao, G. U. Kulkarni, P. J. Thomas, P. P. Edwards. *Chem. Eur. J.* **8**, 28 (2002).
2. C. N. R. Rao, F. L. Deepak, G. Gundiah, A. Govindaraj. *Prog. Solid State Chem.* **31**, 5 (2003).
3. Y. Li, X. Li, C. Yang, Y. Li. *J. Mater. Chem.* **13**, 2641 (2003).
4. Y.-W. Jun, S.-M. Lee, N.-J. Kang, J. Cheon. *J. Am. Chem. Soc.* **123**, 5150 (2001).
5. P. S. Nair, T. Radhakrishnan, N. Revaprasadu, G. A. Kolawole, P. O'Brien. *Chem. Commun.* 564 (2002).
6. C. Qian, F. Kim, L. Ma, F. Tsui, P. Yang, J. Liu. *J. Am. Chem. Soc.* **126**, 1195 (2004).
7. J. Park, B. Koo, K. Y. Yoon, Y. Hwang, M. Kang, J. Park, T. Hyeon. *J. Am. Chem. Soc.* **127**, 8433 (2005).
8. X. Wang, P. Gao, J. Li, C. J. Summers, J. L. Wang. *Adv. Mater*. **14**, 1732 (2002).
9. L. D. Freedman, G. O. Doak. *Chem. Rev.* **57**, 479 (1957).
10. H. Z. Lecher, T. H. Chao, K. C. Whitehouse, R. A. Greenwood. *J. Am. Chem. Soc.* **76**, 1045 (1954).
11. J. McElwee, R. Helmy, A. Y. Fadeev. *J. Colloid Interface Sci.* **285**, 551 (2005).
12. X. G. Peng, L. Manna, W. D. Yang, J. Wickham, E. Scher, A. Kadavanich, A. P. Alivisatos. *Nature* **404**, 59 (2000).
13. M. Kolosky, J. Vialle. *J. Chromatogr.* **299**, 436 (1984).
14. S. D. Scott, H. L. Barnes. *Geochem. Cosmochim. Acta* **36**, 1275 (1972).
15. T. P. Martin. *Phys. Rep.* **273**, 199 (1996).
16. U. Naher, U. Zimmermann, T. P. Martin. *J. Chem. Phys.* **99**, 2256 (1993).
17. J. G. Allpress, J. V. Sanders. *Aust. J. Phys.* **23**, 23 (1970).
18. V. Kumar. *Prog. Crystal Growth Charact.* **34**, 95 (1997).